http://dx.doi.org/10.5012/bkcs.2013.34.7.2073

Preparation of 27$Ni_6Zr_4O_{14}$3M(M=Mg, Ca, Sr, or Ba)O/70 Zeolite Y Catalysts and Hydrogen-rich Gas Production by Ethanol Steam Reforming

Dongjin Kim, Jun Su Lee, Gayoung Lee, Byung-Hyun Choi,† Mi-Jung Ji,† Sun-Min Park,† and Misook Kang*

*Department of Chemistry, College of Science, Yeungnam University, Gyeongsan 712-749, Korea. *E-mail: mskang@ynu.ac.kr*
†Korean Institutes of Ceramic Engineering and Technology (KICET), Geumcheon-gu, Seoul 153-801, Korea
Received February 7, 2013, Accepted April 16, 2013

In this study the effects of adding alkaline-earth (IIA) metal oxides to NiZr-loaded Zeolite Y catalysts were investigated on hydrogen rich production by ethanol steam reforming (ESR). Four kinds of alkaline-earth metal (Mg, Ca, Sr, or Ba) oxides of 3.0% by weight were loaded between the $Ni_6Zr_4O_{14}$ main catalytic species and the microporous Zeolite Y support. The characterizations of these catalysts were examined by XRD, TEM, H_2-TPR, NH_3-TPD, and XPS. Catalytic performances during ESR were found to depend on the basicity of the added alkaline-earth metal oxides and H_2 production and ethanol conversion were maximized to 82% and 98% respectively in 27($Ni_6Zr_4O_{14}$)3MgO/70Zeolite Y catalyst at 600 °C. Many carbon deposits and carbon nano fibers were seen on the surface of 30$Ni_6Zr_4O_{14}$/70Zeolite Y catalyst but lesser amounts were observed on alkaline-earth metal oxide-loaded 27($Ni_6Zr_4O_{14}$)3MO/70Zeolite Y catalysts in TEM photos after ESR. This study demonstrates that hydrogen yields from ESR are closely related to the acidities of catalysts and that alkaline-earth metal oxides reduce the acidities of 27($Ni_6Zr_4O_{14}$)3MO/70Zeolite Y catalysts and promote hydrogen evolution by preventing progression to hydrocarbons.

Key Words : Hydrogen production, Ethanol steam reforming, $Ni_6Zr_4O_{14}$/Zeolite Y, Alkaline-earth (IIA) metal oxides, Acidity

Introduction

Reducing fossil fuel reserves and the pollution caused by continuous energy demands make hydrogen an attractive alternative energy source. The processes for converting petroleum fuels into hydrogen-rich gas products include steam reforming,[1] partial oxidation,[2] auto thermal reforming,[3] dry reforming[4] or combinations of these processes.[5] The production of hydrogen from biomass like methanol and ethanol is receiving increased attention as a potential source of renewable energy given global demands for sustainable energy. In this context, ethanol may represent a potential source for hydrogen production. Ethanol has been used for steam reforming[6,7] because of its non-toxic nature and ease of transport and storage. However, the oxidation temperature of ethanol is higher than that of methanol or dimethyl ether, making its decomposition difficult. Ethanol steam reforming (ESR) offers the advantage of producing more hydrogen per mole from ethanol. Ethanol can be efficiently converted in hydrogen by catalytically reacting it with steam according to the following reaction:

$$CH_3CH_2OH + 3H_2O \rightarrow 6H_2 + 2CO_2,\ \Delta H^o = 207.7\ kJ/mol.$$

Ethanol-reforming reactions include several catalytic steps such as: (i) ethanol dehydrogenation, (ii) carbon-carbon bond breaking of surface intermediates to produce CO and CH_4, and (iii) reaction between water and $\mathbf{C_1}$ intermediate products to generate hydrogen.[8] Ni-based Al_2O_3 support catalysts[9,10] have been used for ordinary steam-reforming processes because of their acceptably activity and significantly lower cost than alternative precious metal-based catalysts. Of the transition metals, the high C–C bond-breaking activity and the relatively low cost of Ni make it a suitable active phase for ethanol-reforming reactions. However, Ni-based Al_2O_3 support catalysts are susceptible to deactivation resulting from the deposition of carbon, even when operating at steam-to-carbon ratios predicted to be thermodynamically outside the carbon-forming regime. An additional serious problem associated with the use of $NiAlO_4$ catalysts is the abrupt catalytic deactivation that occurs at temperatures above 650 °C due to the formation of a $NiAlO_3$ spinal structure resulting from sintering between Ni and Al, which leads to reactor shutdown and the reversal of the feed gases.[11,12] To overcome these problems, many researchers have used non-alumina supported catalysts for ESR applications.[13,14]

In this study, four types of alkaline-earth metal (Mg, Ca, Sr, or Ba) oxides were loaded at 3% by weight onto $Ni_6Zr_4O_{14}$ at 27.0% by weight and then impregnated over a Zeolite Y support (70.0% by weight). It has been revealed[14] that the use of basic additives or promoters that favor water adsorption and OH surface mobility lower the rate of coke deposition on catalyst surfaces. The addition of alkaline earth oxides is widely used in reforming formulations to neutralize the acidity of catalysts. Another approach involves the addition of ZrO_2 to reforming catalysts since this oxide improves the stability of nickel catalysts during the steam reforming.[15,16] In addition, ZrO_2 has high conductivity at high temperature and resists hydrogen reduction and CO poisoning. Thus, we considered that a NiZr-alkaline-earth

metal oxides-loaded Zeolite Y catalyst might improve the oxidation of ethanol into CO and CO_2 by dehydrogenation and that the catalyst would reduce conversion to hydrocarbon intermediates by depressing the acidities of Zeolite Y catalyst.

Experimental

Preparation of $27Ni_6Zr_4O_{14}3M$(M=Mg, Ca, Sr, or Ba)O/70Zeolite Y Catalysts. The four $27Ni_6Zr_4O_{14}3MO$/70Zeolite Y catalysts were obtained using sol-gel and impregnation methods. The procedure used to produce $Ni_6Zr_4O_{14}$ was as follows. $Ni(NO_3)_2$ and $Zr(NO_3)_4$ of purity 99.9% were completely dissolved in distilled water and the mixed solution was stirred homogeneously. Aqueous NH_4OH was slowly dropped into the mixed solution until the pH reached 9.0. The homogeneously mixed solution was evaporated at 80 °C for 6 h to remove water and the precipitate obtained was dried at 50 °C for 24 h and calcined at 500 °C for 2 h in air. In order to prepare $27Ni_6Zr_4O_{14}3MO$, the alkaline-earth metal nitrates, $Mg(NO_3)_2$, $Ca(NO_3)_2$, $Sr(NO_3)_2$, or $Ba(NO_3)_2$ (precursors of Mg, Ca, Sr, or Ba oxides) were each added into four solutions of $Ni_6Zr_4O_{14}$ in ethanol. These slurries were stirring, evaporated, and thermally treated to obtain $Ni_6Zr_4O_{14}$M(M=Mg, Ca, Sr, or Ba)O. Finally, the four types of $Ni_6Zr_4O_{14}$MO and Zeolite Y were mixed in 25.0 mL of ethanol. The slurries obtained were stirred for 2 h, evaporated at 50 °C for 3 h, and heated at 500 °C for 2 h in air. Eventually the five experimental catalysts, that is, the four containing alkaline earth metals and the one without, were prepared as follows, $30Ni_6Zr_4O_{14}$/Zeolite Y, $27Ni_6Zr_4O_{14}3MgO$/70Zeolite Y, $27Ni_6Zr_4O_{14}3CaO$/70Zeolite Y, $27Ni_6Zr_4O_{14}3SrO$/70Zeolite Y, and $27Ni_6Zr_4O_{14}3BaO$/70Zeolite Y. Unlike catalysts previously described[6-16] these catalysts were not reduced with hydrogen gas before ESR.

Characterizations of the $27Ni_6Zr_4O_{14}3M$(M=Mg, Ca, Sr, or Ba)O/70Zeolite Y Catalysts. The five catalysts were subjected to powder X-ray diffraction (XRD; MPD model, PANalytical) analysis using nickel-filtered CuKa radiation (30 kV, 30 mA) at 2-theta angles of 10-100°. Coke growth and catalyst surface atomic compositions after ESR were determined by transmission electron microscopy (TEM; H-7600, Hitachi) and energy dispersive spectroscopy (EDS-EX-250, Horiba), respectively. BET (Brunauer, Emmett, and Teller) surface areas were measured using a Belsorp II instrument. Before BET surface measurements the catalysts were degassed under vacuum at 120 °C for 12 h and surface areas were measured by nitrogen adsorption using a continuous flow method using a mixture of nitrogen and helium as carrier gas. XPS measurement of C_{1s} before and after ESR were recorded using a model ESCALAB250 XPS system (Thermo Fisher Scientific (U.K), Busan Center, Korea Basic Science Institute, Korea) equipped with a non-monochromatic AlKα (1486.6 eV) X-ray source. NH_3-TPD measurements, which were used to determine the acidities of catalysts, were conducted using a conventional TPD system using an N-1000 thermo gravimetric analyzer (TGA; Scinco, Korea). After thermal-treatment at 150 °C under N_2, the samples were exposed to ammonia gas (1.0 mol % ammonia diluted in He) at 80 °C for 30 min and then heated to 600 °C at a heating rate of 10 °C/min. H_2-temperature-programmed reduction (TPR) was conducted using a gas chromatograph (GC series 580, GOW-MAC) equipped with a thermal conductivity detector (TCD), and the analysis of H_2-TPR was carried out under a H_2(10.0 vol %)/N_2 gas flow (30 mL/min) while raising the temperature of the catalyst from room temperature to 700 °C at 5 °C/min. In order to study the formation of carbon species on catalyst surfaces after ESR, temperature-programmed oxidation (TPO) was performed using the TGA N-1000 instrument by introducing high purity oxygen (20-40 mL/min) into the system after purging it with N_2. Coke contents deposited on catalyst surfaces were calculated from weight loss in the temperature range 50 to 900 °C.

The reactor used for ESR was the same as that used in our previous study,[17] and the catalytic activities of the five catalysts were measured in the temperature range 300-800 °C over 1 h at steam-to-ethanol ratio of 1:3 at gas hourly space velocities (GHSV) of 4000 h^{-1}. Catalysts (0.4 g) were pelletized to 20-24 mesh, and to prevent movement were packed with a small amount of quartz wool into a fixed bed quartz reactor, which was vertically mounted inside the furnace. An ethanol/water solution (mol/mol) was then introduced through a vaporizer. The amount of steam was adjusted by regulating the temperature according to the partial pressure law previously described in detail.[17] The flow rate was held constant at 10 and 30 mL/min for ethanol and steam respectively. Argon gas was used to transport the vaporized mixture to the reactor. The products of ESR were identified and quantified using on-line GC (Donam DS6200; Donam company, Korea). The TCD was used to detect H_2, C_2H_5OH, CO, and CO_2 and CH_4 and C_2-C_5 hydrocarbons. Other products were analyzed using the FID detector. Ethanol conversion (XEtOH) and the selectivity of the C-containing products (SC) were calculated using the following equations:

$$X_{EtOH} = (\text{mol EtOH}_{in} - \text{mol EtOH}_{out})/\text{mol EtOH}_{in} \times 100\%$$

$$SC_{H2} = \text{mol } H_2/[(\text{mol EtOH}_{in} - \text{mol EtOH}_{out}) - (\text{mol } H_2O_{in} - \text{mol } H_2O_{out})] \times 100\%$$

$$SC_{others} = \text{mol others}_{out}/(\text{mol EtOH}_{in} - \text{mol EtOH}_{out}) \times 100\%$$

Results and Discussion

Characteristics of the $27Ni_6Zr_4O_{14}3M$(M=Mg, Ca, Sr, or Ba)O/70Zeolite Y Catalysts. The five catalysts, that is, $30Ni_6Zr_4O_{14}$/70Zeolite Y and $27Ni_6Zr_4O_{14}3M$(M=Mg, Ca, Sr, or Ba)O/70Zeolite Y, were characterized by XRD before ESR. XRD patterns are shown in Figure 1. The diffraction lines of the NiO phase at 2-theta angles of 37.27, 43.29, 62.89, 75.44, and 79.43°, corresponding to the (111), (200), (220), (311), and (222) planes, respectively, were seen in the XRD patterns of all catalysts. They were ascribed to the cubic structure and assigned as previously described.[18] The

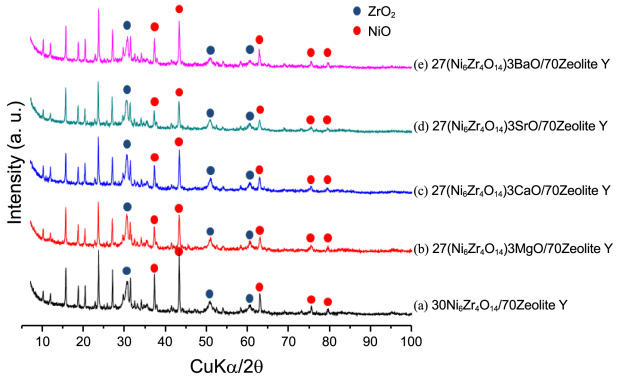

Figure 1. XRD patterns of the five experimental catalysts, one 30Ni$_6$Zr$_4$O$_{14}$/70Zeolite Y and four 27Ni$_6$Zr$_4$O$_{14}$3M(M=Mg, Ca, Sr, and Ba)O/70Zeolite Y, before ethanol steam reforming.

diffraction lines of the ZrO_2 phase at 2-theta angles of around 30.27 (101), 35.24 (110), 50.37 (112), and 60.19° (211) were also exhibited in the XRD patterns of all catalysts, and were assigned to the tetragonal structure (JCPDS card No. 88-1007). All of other peaks emanated from the Zeolite Y support. Unfortunately, no peaks corresponding to the alkaline-earth metal oxides were observed because of the low levels present. However, almost all peaks of the four alkaline earth containing catalysts were smaller than the peaks of 30Ni$_6$Zr$_4$O$_{14}$/70Zeolite Y. The full width at half maximum (FWHM) heights of peaks at 2 theta=43.29° (200) of NiO were measured to determine NiO crystallite sizes. The Scherrer equation in X-ray diffraction and crystallography, is a formula that relates the size of sub-micrometer particles, or crystallites, in a solid to the broadening of a peak in a diffraction pattern; $t = 0.9\lambda/\beta\cos\theta$, where λ is the wavelength of the incident X-rays, β the FWHM in radians and θ is the diffraction angle. Calculated crystallite sizes based on this 43.29° (200) peak were the similar for the four alkaline earth metals containing catalysts at 29-30 nm, whereas that of 30Ni$_6$Zr$_4$O$_{14}$/70Zeolite Y was 42 nm. The smaller crystallite sizes indicated that the NiO was well dispersed on the surface of Zeolite Y support.

In Table 1, EDS analysis (atomic surface composition analysis) revealed variations in loaded alkaline-earth metal concentrations. Atomic compositions determined by EDS reflected surface compositions only. Despite using the same concentrations in the synthesis, the Ni:Zr atomic molar ratios of the five catalysts differed. The presence of ZrO_2 reduces the acidity of the Al_2O_3 support. Concentrations of Mg, Ca, Sr, and Ba in each catalyst were 1.16, 1.20, 1.14, and 1.11 by weight respectively, indicating that the added alkaline earth-metal oxides were similarly distributed over catalyst surfaces. Based on the atomic values of Zr and alkaline metals, Al/(Zr+alkaline metal) ratios which means the amounts of acidities in catalysts exhibited 1.21(30Ni$_6$Zr$_4$O$_{14}$/Zeolite Y), 0.83(27Ni$_6$Zr$_4$O$_{14}$3MgO/Zeolite Y), 0.94 (27Ni$_6$Zr$_4$O$_{14}$3CaO/Zeolite Y), 0.80(27Ni$_6$Zr$_4$O$_{14}$3SrO/Zeolite Y), and 0.76(27Ni$_6$Zr$_4$O$_{14}$3BaO/70Zeolite Y), respectively. Thus, we confirmed that the acidities of 30Ni$_6$Zr$_4$O$_{14}$-3MO/Zeolite Y catalysts decreased according to alkaline earth metal basicity.

Pore size distribution is an important characteristic for porous materials. In this study, we used Zeolite Y as a support. The relative pressure at which pore filling takes place by capillary condensation can be calculated from Kelvin's equation. Using this equation the pore radius in which capillary condensation occurs actively can be determined as a function of the relative pressure (P/P_0). Mean pore diameter D_p was calculated using $D_p = 4VT/S$ where VT is the total volume of pores and S the BET surface area.

Figure 2 and Table 2 show the adsorption-desorption isotherms of N_2 at 77 K for the five catalysts. They illustrate the N_2 adsorption isotherms for the microporous materials induced from Zeolite Y support. All isotherms belonged to I type of the IUPAC classification[19] for all samples. The isotherms were wide without any clear plateau and a certain hysteresis slope was observed at intermediate and high relative pressures for all five catalysts, which is indicative of the presence of large micropores in Zeolite Y. The adsorption and desorption lines for the five experimental catalysts overlapped completely in the low relative pressure range while the hysteresis loop was in the high relative pressure region (P/P_0 0.5-1.0), mainly because of the presence of pores. In Table 2, the average pore diameter values D_p ranged from 0.34 to 0.43 nm for all catalysts and the pore sizes decreased with additions of alkaline earth metal oxides. Generally, the cavity size in pure Zeolite Y was 0.74 nm, but the pores seemed to be partially blocked by NiO and ZrO_2 in all catalysts studies. The BET surface areas of the four alkaline earth containing Zeolite Y catalysts were much lower than the 517.07 m^2/g of the 30Ni$_6$Zr$_4$O$_{14}$/70Zeolite Y catalyst and their surface areas were in the range 288-324 m^2/g. The total volumes of all catalysts showed the same tendencies as their surface areas.

To determine the relation between catalytic performance

Table 1. Atomic compositions calculated by EDS analysis of the five catalysts, one 30Ni$_6$Zr$_4$O$_{14}$/70Zeolite Y and four 27Ni$_6$Zr$_4$O$_{14}$3M (M=Mg, Ca, Sr, and Ba)O/70Zeolite Y

Catalysts \ Elements (atomic ratio)	O	Ni	Zr	Si	Al	Mg, Ca, Sr, Ba
a) 30Ni$_6$Zr$_4$O$_{14}$/70Zeolite Y	43.67	3.79	6.84	10.06	8.24	-
b) 27(Ni$_6$Zr$_4$O$_{14}$)3MgO/70Zeolite Y	56.50	3.00	5.07	10.75	5.18	1.16
c) 27(Ni$_6$Zr$_4$O$_{14}$)3CaO/70Zeolite Y	48.47	3.32	3.82	11.91	4.75	1.20
d) 27(Ni$_6$Zr$_4$O$_{14}$)3SrO/70Zeolite Y	52.52	3.51	4.58	12.81	4.62	1.14
e) 27(Ni$_6$Zr$_4$O$_{14}$)3BaO/70Zeolite Y	61.28	3.25	6.32	16.56	5.65	1.11

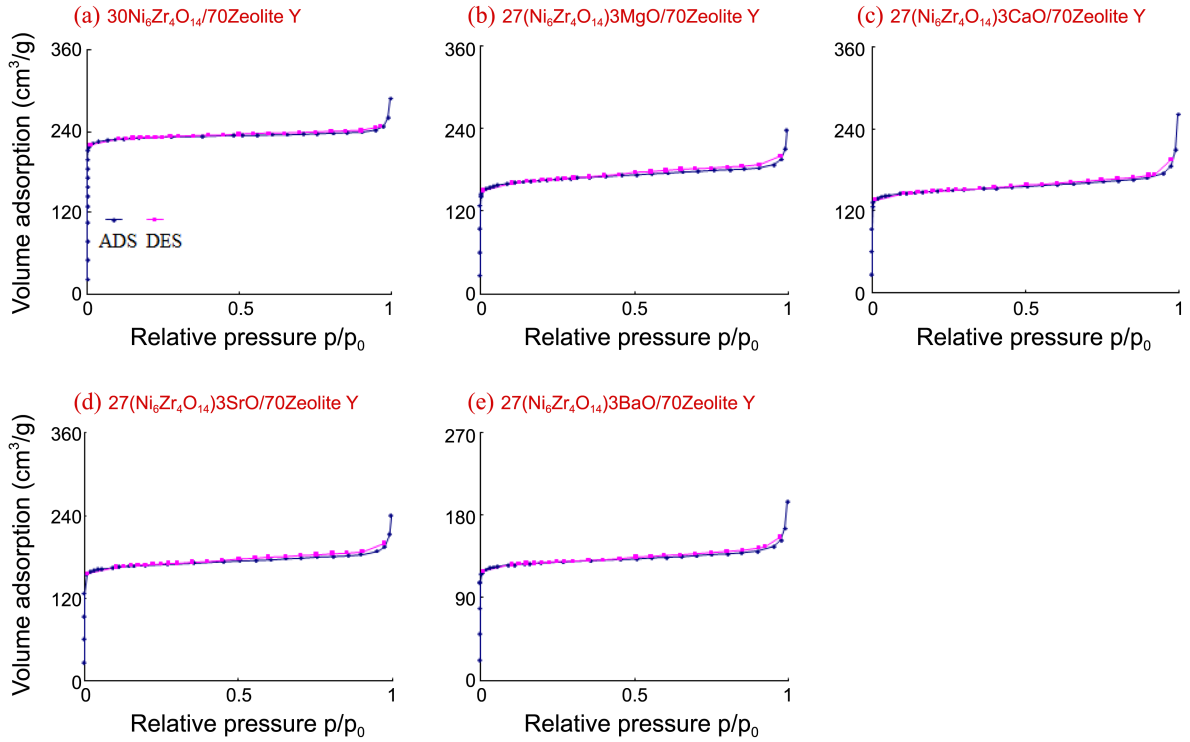

Figure 2. Adsorption-desorption isotherm curves of the five experimental catalysts, one $30Ni_6Zr_4O_{14}$/70Zeolite Y and four $27Ni_6Zr_4O_{14}3M$ (M=Mg, Ca, Sr, and Ba)O/70Zeolite Y.

Table 2. BET surface areas and pore diameters determined using adsorption-desorption isotherm curves for the five experimental catalysts, one $30Ni_6Zr_4O_{14}$/70Zeolite Y and four $27Ni_6Zr_4O_{14}3M$(M=Mg, Ca, Sr, and Ba)O/70Zeolite Y

Elements / Catalysts	BET Surface area (m^2g^{-1})	Total Pore Volume (cm^3g^{-1})	Pore Diameter (nm)
a) $30Ni_6Zr_4O_{14}$/70Zeolite Y	517.07	0.44	0.43
b) $27(Ni_6Zr_4O_{14})3MgO$/70Zeolite Y	324.92	0.28	0.35
c) $27(Ni_6Zr_4O_{14})3CaO$/70Zeolite Y	288.88	0.31	0.34
d) $27(Ni_6Zr_4O_{14})3SrO$/70Zeolite Y	309.24	0.27	0.35
e) $27(Ni_6Zr_4O_{14})3BaO$/70Zeolite Y	296.23	0.30	0.35

and Brfnsted acidic properties, the NH_3-TPD profiles of the five catalysts were obtained (Figure 3). Solid catalytic materials possess many acid sites and acidic strengths that are attributed to their high Al contents. In general, the NH_3-TPD profiles of porous catalysts consist of two peaks: one in the low temperature range of 150-250 °C and the other in the high temperature range of 350-450 °C. These low and high NH_3-desorption peaks correspond to weak and strong acid sites respectively.[20] In Figure 3, all five catalysts had a peak at a temperature of around 150 °C, which was attributed to the presence of Al in Zeolite Y. During ESR the oxidation of carbon oxides by oxygen from injected water, and hydrocarbon generation by protons at medium Brfnsted acid sites occur simultaneously. The latter reaction affects the absolute performance of the catalyst. Consequently, more strong acid sites in the support promote the dehydration of ethanol to ethylene, which results in the generation of longer chained hydrocarbon cokes. One significant point was that shifts in acid sites to low temperature occurred with the addition of

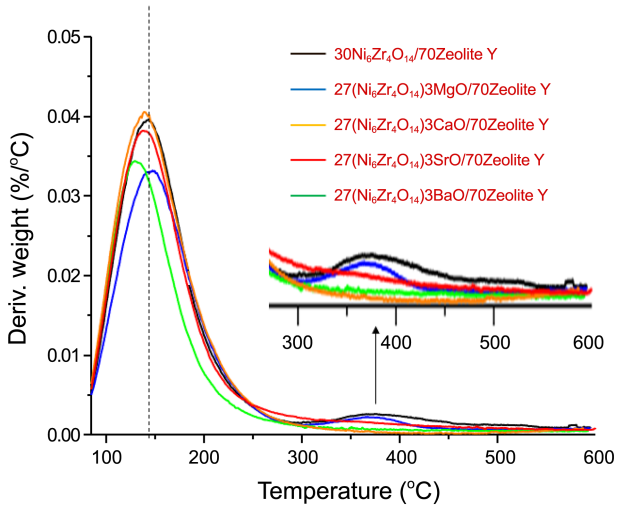

Figure 3. NH_3-TPD curves of the five experimental catalysts, one $30Ni_6Zr_4O_{14}$/70Zeolite Y and four $27Ni_6Zr_4O_{14}3M$(M=Mg, Ca, Sr, and Ba)O/70Zeolite Y.

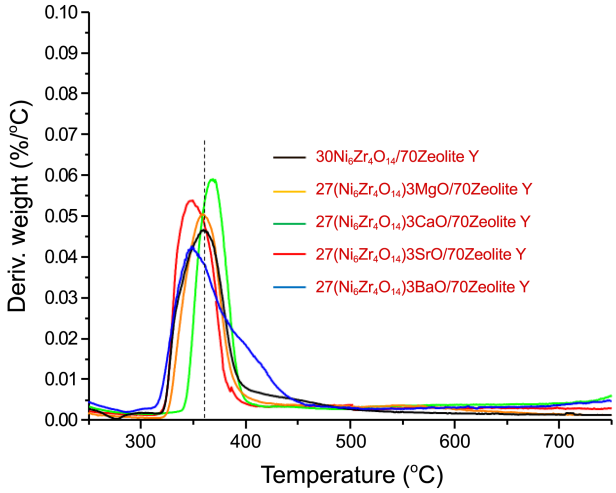

Figure 4. H_2-TPR curves of the five experimental catalysts, one $30Ni_6Zr_4O_{14}$/70Zeolite Y and four $27Ni_6Zr_4O_{14}3M$(M=Mg, Ca, Sr, and Ba)O/70Zeolite Y.

the alkaline-earth metal oxides and acidity was much reduced for the $27Ni_6Zr_4O_{14}3BaO$/70Zeolite Y catalyst. In addition, acidity was almost absent for Sr and Ba-loaded NiZr/Zeolite Y catalysts. This tendency was the same as that observed for Al/(Zr+alkaline metal) ratio by EDS analysis. Thus, this result shows that the acidities of catalysts were dependent on the basicities of the added alkaline-earth metal oxides.

The H_2-TPR profiles of the five catalysts are shown in Figure 4. Changes corresponding to the reductions of NiO/Ni ratio were observed in H_2-TPR profiles. However, the reduced peaks for ZrO_2 and alkaline metal oxides are not shown because their reductions are probably difficult (the reduction potential values of negative charges have). In general, H_2-TPR results indicated that the peak areas corresponded to hydrogen uptake and the peak at high temperatures corresponds to the catalytic reaction involved in the reduction. A reduction type for NiO was seen in all four catalysts at 300-400 °C, which was considered to be due to NiO to Ni transition. The reduction peak of NiO was gradually shifted to lower temperatures with the addition of alkaline-earth metal oxides, except CaO, and the greatest reduction was observed for $27Ni_6Zr_4O_{14}3SrO$/70Zeolite Y. This result was attributed that the alkaline-earth metal oxides could help reduction of NiO to Ni^0. These properties can probably promote ethanol dehydration over Ni during ESR.

ESR Over the Five Experimental Catalysts. ESR was carried out using 0.5 g of each of the five catalysts under the reaction conditions 300-800 °C, GHSV 4000 h^{-1}, and H_2O/EtOH ratio 3.0. Figure 5 compares the activities of the five catalysts at various temperatures. ESR reactions include several catalytic steps, that is, ethanol dehydrogenation, carbon-carbon bond breaking of surface intermediates to produce CO and CH_4, and water reforming of the C_1 intermediate products to generate hydrogen. The following summarized the reaction pathways that constitute ESR over metal catalysts.

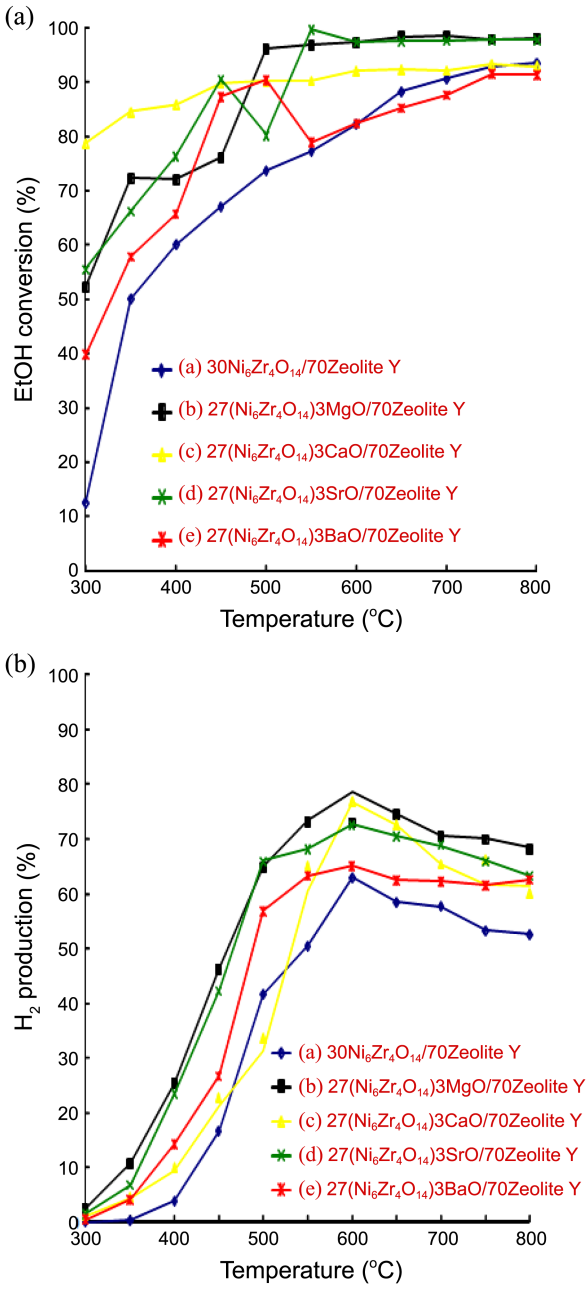

Figure 5. H_2 production (a) and ethanol conversion (b) over the five experimental catalysts at different reaction temperatures.

$$2CH_3CH_2OH \rightarrow CH_3CH_2OCH_2CH_3 + H_2O \quad (1)$$

$$CH_3CH_2OCH_2CH_3 + \text{acid } H^+ \rightarrow C_2H_4 + CH_3CH_2OH \quad (2)$$

$$CH_3CH_2OH \rightarrow CH_3CHO + H_2 \quad (3)$$

$$CH_3CH_2OH + \text{acid } H^+ \rightarrow C_2H_4 + H_2O \quad (4)$$

$$CH_3CHO \rightarrow CH_4 + CO \quad (5)$$

$$CH_3CHO + H_2O \rightarrow 2CO + 3H_2 \quad (6)$$

$$CH_4 + H_2O \rightarrow CO + 3H_2 \quad (7)$$

$$CO + H_2O \rightarrow CO_2 + H_2 \quad (8)$$

$$C_2H_4 + \text{acid } H^+ \rightarrow\rightarrow\rightarrow \text{Carbon} \quad (9)$$

The two main reaction pathways for ESR are the dehydration and dehydrogenation routes. Catalyst type has a

significant impact on the reaction pathway and the product s obtained. The most important thing in this study was that large amount of acid sites in the supports promoted the dehydration of ethanol to ethylene and coke formation (steps 2, 4, and 9 above). Only ethanol conversion in Figure A) was compared and the Conversion over the $27Ni_6Zr_4O_{14}3MgO$/70Zeolite Y catalyst was higher than over the other four catalysts, and reached 98% at 500 °C. Hydrogen productions also gradually increased over all catalysts from 350 to 600 °C and reached a maximum of 82% at 600 °C over $27Ni_6Zr_4O_{14}3MgO$/70Zeolite Y. The alkaline-earth metal oxide-loaded catalysts had significantly higher reforming reactivity than the NiZr-based catalyst. Additionally the ESR reaction was further improved at low temperature and the activation point was shifted to lower temperature in the $27Ni_6Zr_4O_{14}3M$(M=Mg, Ca, Sr, or Ba)O/70Zeolite Y catalysts. These results suggest that the alkaline earth-metal oxides prevented sintering between the Ni particles and hindered both ethanol dehydration and ethylene formation related to coking by reducing catalyst acidity. However, the mechanism also indicates that though some acidity (Brfnsted) is necessary too much causes catalytic deactivation. In addition, H_2 production for $27Ni_6Zr_4O_{14}3MgO$/70Zeolite Y in figure B) was positively correlated with GHSV when the reaction temperature exceeded 350 °C with an ethanol conversion exceeding 90% over the entire GHSV range. The efficiencies of ethanol conversion and hydrogen production were both reduced when GHSV decreased below 3000 and increased over the complete temperature range when GHSV exceeded 6000 h^{-1}. Under optimal conditions corresponding to an EtOH: H_2O ratio of 3:1, 85% of hydrogen was emitted at 600 °C and the ethanol conversion was 98%.

Characteristics of Catalysts After Ethanol Steam Reforming. Figure 6 compares the XRD patterns of the five catalysts after 10 h of reaction at 600 °C. The diffraction

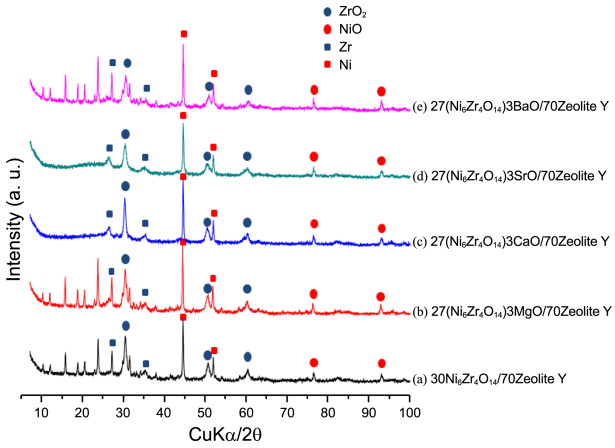

Figure 6. Comparison of XRD patterns of the five experimental catalysts before and after ethanol steam reforming.

lines of the Ni metal phase at 2-theta angles of 44.49° (111) and 51.85° (420) [JCPDS#87-0712] were clearly different after ESR for all five catalysts and the peaks assigned to NiO were smaller. This finding indicated that the Ni ingredients acted as active sites during ESR (in the ESR mechanism mentioned above, steps 3, 5, 7, and 8 all occur over NiO, which is reduced to Ni during ESR. The Zeolite Y frameworks seemed to be destroyed in $27Ni_6Zr_4O_{14}3CaO$/70Zeolite Y and $27Ni_6Zr_4O_{14}3SrO$/70Zeolite Y catalysts after ESR, which was probably associated with aggregation due to their low dispersions over the Zeolite Y support. On the other hand, Zr metal phases appeared after ESR at 2-theta angles of 25.44° (110) and 35.78° (110) [JCPDS #34-0657] and this trend was particularly pronounced in $27Ni_6Zr_4O_{14}3MgO$ and BaO/70Zeolite Y catalysts. In step 8) step of the CO oxidation mechanism, ZrO_2 also acts as a catalytic species. This result confirms that MgO also aids ESR like Ni and Zr.

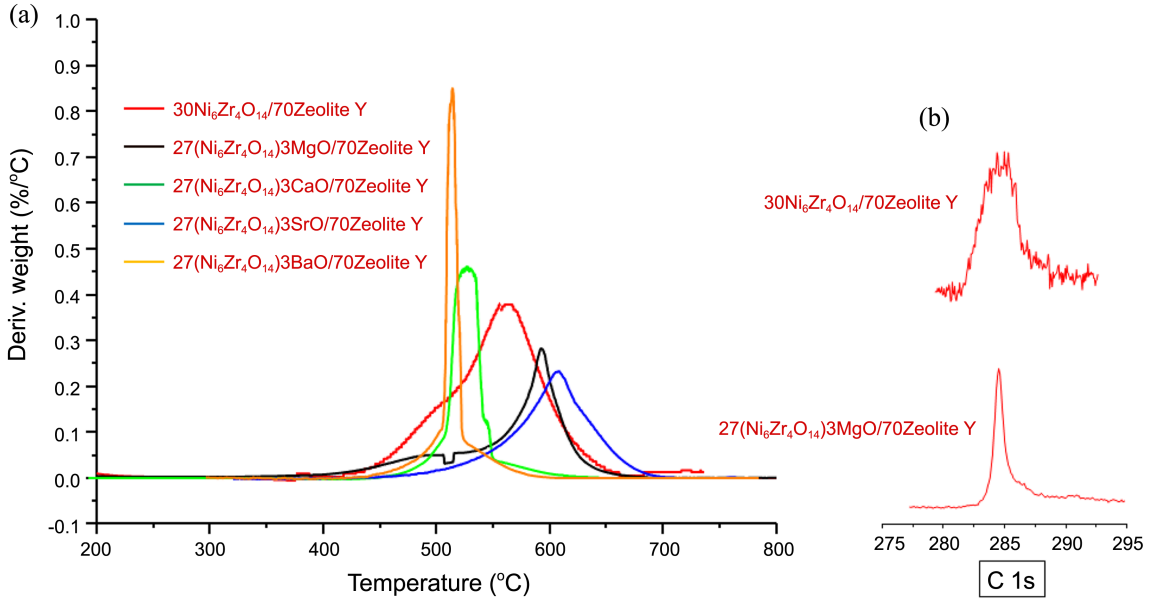

Figure 7. TPO profiles (a) and XPS curves (b) of the C1s of the five experimental catalysts after ethanol steam reforming.

To determine the amount of carbon deposited on catalysts after ESR, we carried out TPO measurements (A) and C1s XPS analysis (B) as shown in Figure 7. Deposited amounts (peak area) and carbon species (decomposition temperature) are closely related to catalytic deactivation. Generally, the extent of catalytic deactivation is lower when smaller amounts of carbon are deposited. When 30$Ni_6Zr_4O_{14}$/70Zeolite Y was used, deposited carbon exhibited greater oxidation at 560 °C indicating the deposition of longer chain carbons. Carbon oxidations at lower temperature were observed for 27$Ni_6Zr_4O_{14}$3CaO/70Zeolite Y and 27$Ni_6Zr_4O_{14}$3BaO/70Zeolite Y catalysts and peak areas were smaller than those on the other catalysts in both. Carbons deposited on 27$Ni_6Zr_4O_{14}$3MgO/70Zeolite Y and 27$Ni_6Zr_4O_{14}$3SrO/70Zeolite Y were oxidized at slightly higher temperatures and were present in smaller amounts. Therefore, we concluded that the alkaline earth-metal oxides helped to retain the thermal stability of the NiO and to inhibit aggregation during ESR, and that this was responsible for the better stability of the four alkaline earth containing catalysts. Additionally the alkaline-earth metal oxides in the NiZr/Zeolite Y catalysts possibly hindered ethanol dehydration and ethylene formation related to coking, and improved catalytic activity. On the other hand although one C1s orbital was generally seen at 284.5 eV for bulky carbons,[21] the peak presented in this study was split into three peaks at 281.0, 283.2-284.8, and 288.2 eV due to the mixtures of carbide, carbon, and carboxyl species in deposited coke on the 30$Ni_6Zr_4O_{14}$/70Zeolite Y catalyst. However, a sharp peak, indicative of a single carbon entity, was observed in the C1s orbital of 27$Ni_6Zr_4O_{14}$3MgO/70Zeolite Y.

One interesting result shown in Figure 8 was that the carbon deposits on the five catalysts were observed by TEM after ESR. After ESR for 10 h at 600 °C carbon deposited were observed on the surface of five catalysts. As we suggested above, a molecule of ethanol was dissolved into two molecules of CO and H_2 and was subsequently converted at higher temperatures to pure carbon. The hydrogen and oxygen may have disappeared due to reaction with metal oxides in the absence of any kind of metal or functioning catalyst. Finally the carbons react with H_2 and are transferred into C=C molecules (C_2H_4) which can act as precursors of carbon nano-filaments or tubes,[22] as may be inferred from CH_4 evolution during ethanol cracking. Interestingly many carbon deposits formed on alkaline earth containing 30$Ni_6Zr_4O_{14}$/70Zeolite Y catalysts. Furthermore, carbon nanofiber amounts increased with increasing alkaline-earth metal oxide basicity. Generally, the C_2H_4 could be converted into carbon nanofibers in a H_2 atmosphere on a Ni-based catalyst surface. In the present study, alkaline-earth metal oxides helped stabilize

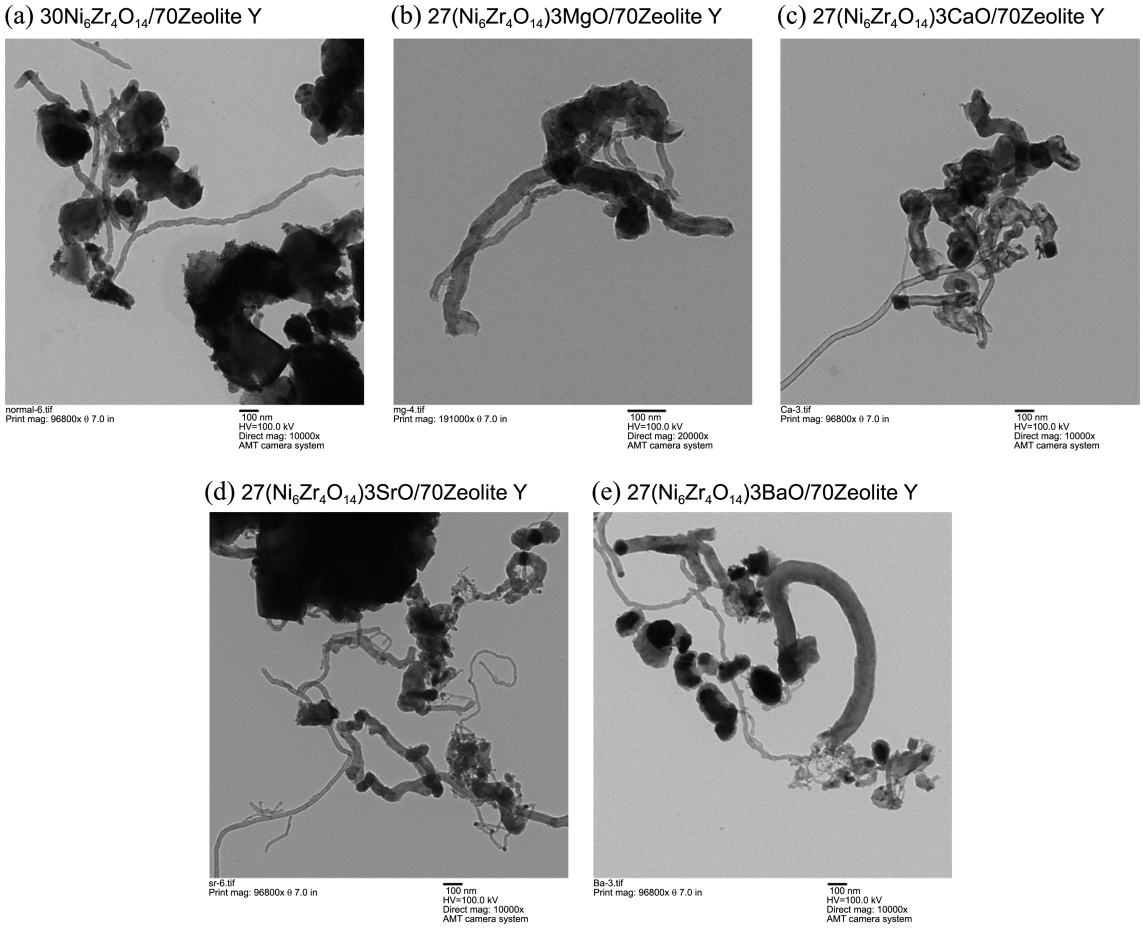

Figure 8. TEM images of deposited carbon over the five experimental catalysts after ethanol steam reforming.

the NiO at high temperatures and extend its catalytic activity, which eventually led to the formation of many carbon nanofibers. However the total amounts of carbon deposited decreased in the order of alkaline earth oxide basicity, that is, non-loaded > MgO-loaded > CaO-loaded > SrO-loaded > BaO-loaded.

Conclusions

The two important points raised by this study are the positive effects alkaline-earth metal oxides have on H_2 rich-production by NiZr-loaded Zeolite Y catalysts and their inhibitory effects on catalytic deactivation. Based on observed performances and the physical measurements made, we proposed that alkaline-earth metal oxides aid the oxidation of feed gases and depressing sintering between Ni particles and the hydrocarbon production during ESR, and that these effects retard catalytic deactivation. Consequently, the alkaline-earth metal oxides increased ethanol conversion and H_2 production for the $27Ni_6Zr_4O_{14}3MgO/70$Zeolite Y catalyst to 98% and 82% respectively at a reaction temperature of 600 °C, a GHSV of 4000 h^{-1}, and an ethanol: H_2O feed ratio of 1:3. We believe that this result is attributable to a decrease of catalyst acidity and a reduction in crystallite sizes of active species, since carbon formation occurs mainly when metal clusters are greater than a critical value.

Acknowledgments. This work was supported by New & Renewable Energy of the Korea Institute of Energy Technology Evaluation and Planning (KETEP) grant funded by the Korea Ministry of Knowledge Economy (No. 2010T100100622).

References

1. Vizcaino, A. J.; Lindo, M.; Carrero, A.; Calles, J. A. *Inter. J. Hydrogen Energy* **2010**, *37*, 1985.
2. Al-Hamamre, Z.; Hararah, M. A. *Inter. J. Hydrogen Energy* **2010**, *35*, 5367.
3. Youn, M. H.; Seo, J. G.; Song, *Inter. J. Hydrogen Energy* **2010**, *35*, 3490.
4. Wang, W.; Wang, Y. *Inter. J. Hydrogen Energy* **2009**, *34*, 5382.
5. Jing, Q.; Lou, H.; Mo, L.; Fei, J.; Zheng, Z. J. *Mol. Catal. A: Chem.* **2004**, *212*, 211.
6. Lindo, M.; Vizcaino, A. J.; Calles, J. A.; Carrero, A. *Inter. J. Hydrogen Energy* **2010**, *35*, 5895.
7. Nageswara, R. P.; Anamika, M.; Deepak, K. *Chem. Eng. J.* **2011**, *167*, 578.
8. Prakash, D. V.; Alirio, E. R. *Chem. Eng. J.* **2006**, *117*, 39.
9. Bang, Y.; Seo, J. G.; Song, I. K. *Inter. J. Hydrogen Energy* **2011**, *36*, 8307.
10. Gabriella, G.; Alberto, L.; Paola, R.; Guido, B. *Appl. Catal. B: Environ.* **2013**, *129*, 460.
11. Xiang, L.; Gong, Y. L.; Li, J. C.; Wang, Z. W. *Appl. Surf. Sci.* **2004**, *239*, 94.
12. Borowiecki, T.; Denis, A.; Gac, W.; Dziembaj, R.; Piwowarska, Z.; Drozdek, M. *Appl. Catal. A: Gen.* **2004**, *274*, 259.
13. Vizcaino, A. J.; Carrero, A.; Calles, J. A. *Inter. J. Hydrogen Energy* **2007**, *32*, 1450.
14. Prakash, B.; Deepak, K. *Inter. J. Hydrogen Energy* **2007**, *32*, 969.
15. Li, S.; Li, M.; Zhang, C.; Wang, S.; Ma, X.; Gong, J. *Inter. J. Hydrogen Energy* **2012**, *37*, 2940.
16. Llenia, R.; Cerare, B.; Claudia, L. B.; Valentina, N.; Michela, S.; Federica, M.; Elisabetta, F.; Gianguido, R.; Alessandro, D. M. *Appl. Catal. B: Environ.* **2012**, *117-118*, 384.
17. Kwak, B. S.; Kim, J.; Kang, M. *Inter. J. Hydrogen Energy* **2010**, *35*, 11829.
18. Sun, J.; Qiu, T.; Wang, J.; Liu, H.; Yang, W. *Mater. Lett*., in press.
19. Sangwichien, C.; Aranovich, G. L.; Donohue, M. D. *Colloids. Surf. A: Physicochem. Eng. Aspects* **2002**, *206*, 313.
20. Zhang, W.; Burckle, E. C.; Smirniotis, P. G. *Micropor. Mesopor. Mater*. **1999**, *33*, 173.
21. Tressaud, A.; Durand, E.; Labrugere, C. J. *Fluorine Chem.* **2004**, *125*, 1639.
22. Li, Y.; Li, D.; Wang, G. *Catal. Today* **2011**, *162*, 1.